10 kHz repetitive high-resolution TV Thomson scattering on TEXTOR: Design and performance (invited)

H. J. van der Meiden, S. K. Varshney, C. J. Barth, T. Oyevaar, R. Jaspers, and A. J. H. Donné[a)]
FOM-Institute for Plasma Physics Rijnhuizen,[b), c)] Association EURATOM-FOM, P.O. Box 1207, 3430 BE Nieuwegein, The Netherlands

M. Yu. Kantor and D. V. Kouprienko
Ioffe Institute, RAS, Saint Petersburg 194021, Russia

E. Uzgel, W. Biel, A. Pospieszczyk, and TEXTOR Team
Institut für Plasmaphysik, Forschungszentrum Jülich,[c)] EURATOM Association, D-52425 Jülich, Germany

(Received 2 May 2006; presented on 8 May 2006; accepted 11 June 2006; published online 4 October 2006)

In late 2003 a 10 kHz multiposition Thomson scattering diagnostic with high spatial resolution became operational on the TEXTOR tokamak. In the initial phase of operation, one burst of 18 pulses of 12 J each with a repetition rate of 5 kHz could be extracted from the laser system. The installation of a low-dope ruby rod (spring 2005) resulted in a system, which can deliver higher pulse energy and moreover a divergence of better than 0.7 mrad, leading to a big improvement in the detection of Thomson scattering photons. Furthermore, the number of laser pulses in one burst could be extended to even more than 30. The achieved laser energy of more than 15 J/pulse makes it possible to measure electron temperature and density profiles with an observational error of 8% on the electron temperature (T_e) and 4% on the electron density (n_e) at $n_e=2.5\times10^{19}$ m^{-3}, per spatial element of 7.5 mm. The viewing optics enables sampling of either the full plasma diameter of 900 mm with 120 spatial channels of 7.5 mm each or a 160 mm long edge chord with 98 spatial channels of 1.7 mm each. The system, which has recently become available for physics exploration, has already been used to study the structure of $m=2$ magnetic islands and the response of the plasma to off-axis electron cyclotron resonance heating. © *2006 American Institute of Physics.*
[DOI: 10.1063/1.2219434]

I. INTRODUCTION

The development of TV-like detectors paved the way to the design of a relatively simple and smart setup to measure simultaneously the electron temperature (T_e) and density (n_e) in plasmas at many positions along a laser chord, using a single laser pulse. The multiposition Thomson scattering (TS) system based on such a TV-like detector was built for Princeton Large Tokamak in 1978.[1] The development of TV Thomson scattering (TVTS) systems got a new impulse in 1994 by the introduction of a high-resolution TVTS system on the Rijnhuizen Tokamak Project.[2] Double-pulse versions of this system were installed on the TJ-II stellarator[3] and the TEXTOR tokamak.[4]

The double-pulse TVTS system at the TEXTOR tokamak ($R_0=1.75$ m, $a=0.46$ m, $B_0<2.9$ T, and $I_p<0.8$ MA) operated successfully from 2000 until 2001. This TS system was based on a double-pulse ruby laser (2×12 J) and two intensified charge coupled device (CCD) cameras for recording the scattered light. It was capable of measuring two T_e and n_e profiles during one discharge along a vertical chord of 900 mm length (at $R=1.84$ m) with 120 spatial channels of 7.5 mm each.

To study the dynamics of mesoscale structures like magnetohydrodynamic (MHD) islands and internal transport barriers in hot plasmas, one needs a repetitive system with a time resolution of <1 ms. Therefore, a TS system is developed. It consists of a repetitive laser and a fast detection system. The Ioffe Institute in St. Petersburg and MultiTech

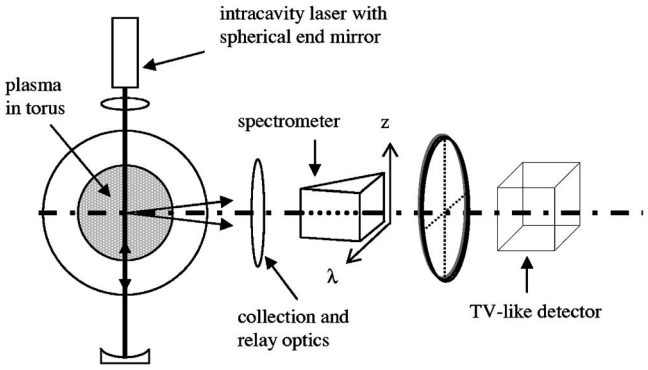

FIG. 1. Schematic overview of the TEXTOR TVTS system with intracavity ruby laser. The collected scattered light is relayed to a Littrow spectrometer giving a two-dimensional (2D) image (λ,z), which is projected onto the cathode of a TV-like detector.

[a)]Electronic mail: donne@rijnh.nl
[b)]URL: http//www.rijnh.nl
[c)]Partners in the Trilateral Euregio Cluster.

Ltd. designed and constructed a so-called double-pass intracavity laser.[4,5] The system is operating like a normal laser oscillator; however, in this case the plasma is part of an 18 m long cavity. To preserve the high spatial resolution of the diagnostic, as well as to adapt as much as possible to the existing viewing optics, the beam path of the new laser is kept the same as that of the double-pulse laser. A state of the art detector has been constructed based on two 12 bit Phantom V7.0 complementary metal oxide semiconductor (CMOS) cameras and a special image intensifier stage.

In this article the design aspects of the multipulse TVTS system (MPTS) for TEXTOR are described in Secs. III and IV, starting with an overview of the multipulse TS system in Sec. II. The achieved system performance and earlier results are presented in Secs. V–VIII.

II. BASIC OVERVIEW OF THE MPTS SYSTEM

The basic setup of the TEXTOR multipulse TVTS system is shown in Fig. 1. Basically, the layout of the system is comparable to that of the previous double-pulse system. The main difference is the use of (1) a multipulse intracavity ruby laser instead of a double-pulse conventional ruby laser and (2) an ultrafast multiframe detector instead of a combination of two single-frame intensified CCD cameras.

In the intracavity setup the plasma is included in the laser cavity, and the laser beam travels many times back and forth through the scattering volume, giving a higher laser efficiency than is the case for a conventional laser. This photon-recycling setup enables the generation of a long train of pulses; moreover, the energy of each individual pulse is typically higher than that produced by conventional high power lasers.

Scattered light is collected by a multielement viewing lens and relayed to a spectrometer by coherent fiber bundles (not drawn in Fig. 1). Either the full plasma diameter of 900 mm with 120 spatial channels of 7.5 mm each or a 160 mm long edge chord with 98 spatial channels of 1.7 mm each can be sampled.

Spectral analysis is performed by a spectrometer in Littrow configuration, covering a spectral range of 585–800 nm (for the full chord observation). The two-dimensional intermediate image (λ, z) is projected onto the highly sensitive cathode of a gated image intensifier. The amplified light is recorded by two fast CMOS cameras (only one is drawn in Fig. 1). This camera was selected because of its high recording frame rate of 10 900 frames/s at an image format of 512×384 pixels and a 12 bit dynamic range.

III. MULTIPULSE INTRACAVITY LASER

At the Ioffe Institute comprehensive research has been performed on intracavity laser systems. The collaboration between this institute and FOM Rijnhuizen resulted in the development of a so-called double-pass intracavity laser with a cavity length of 18 m, as shown in Fig. 2.[6] Here, the laser beam passes twice through the plasma along exactly the same path before returning again into the lasing medium. The basic elements of the intracavity laser are similar tothose of an established laser oscillator. Between the flat rear mirror

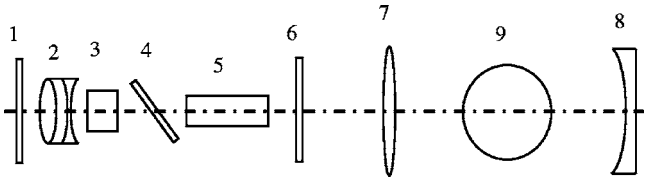

FIG. 2. Double-pass intracavity system with active Q switch: (1) rear mirror, (2) objective, (3) Q switch, (4) polarizer, (5) ruby rod, (6) glass plate, (7) focusing lens, (8) spherical mirror, and (9) plasma volume.

and the active medium (0.05% Cr^+ ruby rod of 19 mm diameter and 200 mm length) an objective (item 2) controls the beam quality by compensating effects of thermal lensing in the ruby rod. The number of extracted pulses can be controlled by the Q switch (item 3). The combination of the rear mirror (item 1) and the glass plate (item 6) form a short cavity to initiate laser operation. The laser beam is focused into the plasma by a lens system (item 7) and returned into the active medium by a spherical mirror (item 8).

In Fig. 3 a train of 20 laser pulses is shown, produced by the double-pass intracavity system using a saturable absorber as a passive Q switch. The application of a saturable absorber results in an irregular pulse separation, which is not preferred for systematic research of fast plasma phenomena. Therefore, an intracavity laser based on active Q switching using a Pockels cell in combination with a polarizer has been developed. The main advantage of the active Q switch is the programmable (and, hence, more regular) time separation between pulses and, in combination with a special power supply, the possibility to extend the pulse train up to 40 pulses or more.

The final version of the double-pass intracavity laser system is installed inside the TEXTOR bunker.[7] Both the focusing telescope (item 7) and the spherical mirror have a focal length of 4.5 m, corresponding to the length of the entrance and exit tubes connected to the TEXTOR torus. The lens is at about 9 m distance from both cavity mirrors, which makes the system less sensitive to misalignment. The beam diameter at the input and output windows is ~25 mm, thus limiting the power density well below the damage threshold of 250 MW/cm^2.

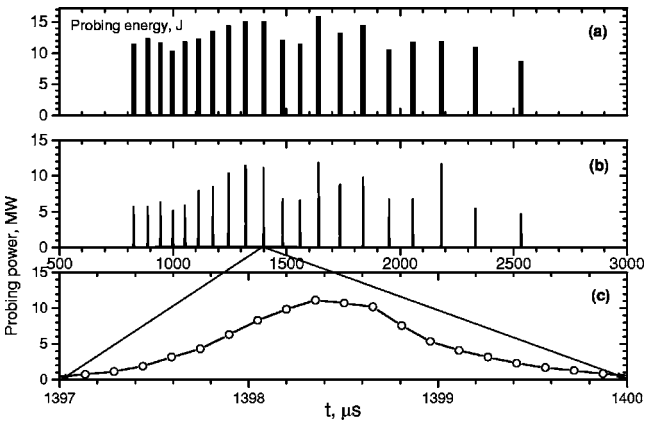

FIG. 3. A train of 20 laser pulses produced by the double-pass intracavity system with an 80% saturable absorber as passive Q switch, yielding a total probing energy of ~200 J.

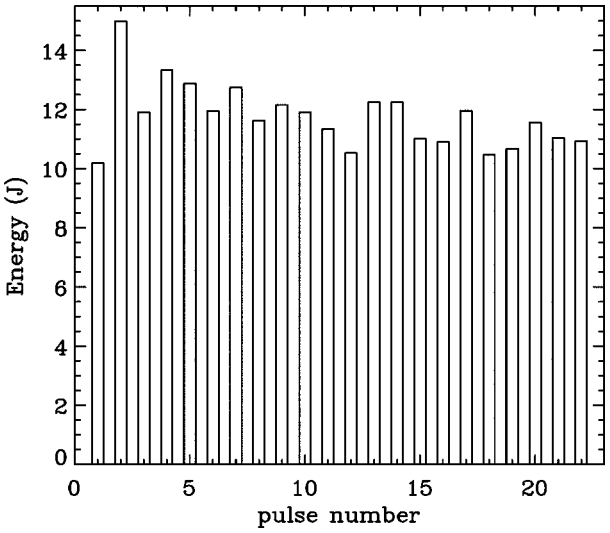

FIG. 4. Intracavity laser operation at 5 kHz and at medium flash lamp power, using a 0.03% Cr^+ doped ruby rod (TEXTOR shot 100194).

The 0.05% Cr^+ ruby rod is pumped by six flash tubes. Each lamp is supplied with ~0.5 MW pumping power which is kept constant during the burst duration of typically 5–10 ms. To obtain a block wave for the pumping voltage a special power supply has been designed and constructed by MultiTech Ltd. in St. Petersburg.

Using an active Q switch at a repetition rate of 5 kHz, a total probing energy of ~236 J in one burst of pulses was achieved.[7] The full width at half maximum (FWHMs) of the laser pulses are 1–1.5 μs. Taking into account the cavity length of 18 m the laser light travels, within this time corresponding to the pulse width, about 23 times up and down through the scattering volume. In other words each laser pulse within a burst has a microstructure of smaller laser pulses each with an average energy of ~0.6 J. The microstructure is, however, not observed by the detection system, which only observes the integrated laser pulse with total energy of ~15 J. The word "pulse" in this article therefore refers to the integrated laser pulse. Although high probing energies are achievable with this setup, luminescence measurements at the ruby-rod cross section indicated that the amplification process in the 0.05% Cr^+ ruby rod occurs predominantly at the periphery. It is obvious that thermal-lensing effects will occur, preventing the laser to operate with stable and low divergences. The same effect caused the pulse energy to decrease from 15 J for the first pulses to 5–8 J for the later pulses in the burst.

To reduce this effect, the intracavity system was equipped in 2005 with a 0.03% Cr^+ ruby rod, resulting in a laser beam divergence of less than 0.7 mrad. In Fig. 4 a burst of pulses is shown for the low-dope ruby rod case. Although the flash lamp power was limited for lifetime considerations, a pulse train consisting of 22 pulses with average pulse energies of 10–12 J could be easily generated, without any strong degradation of pulse energy within the burst. Higher power levels up to 15 J have also been reached in trains with up to 14 – 15 pulses. For comparison photographs of burn spots are shown in Figs. 5(a) and 5(b), corresponding to laser operation with a high- and low-dope ruby rod, respectively.

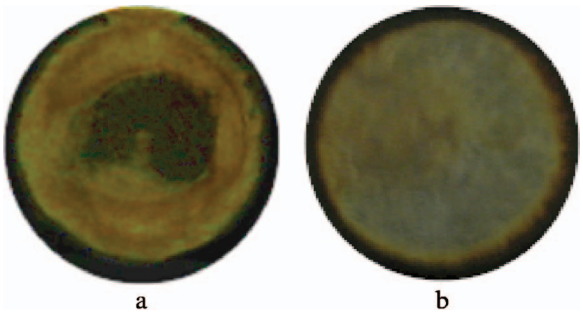

FIG. 5. (Color) (a) Burn spot measured in the vicinity of the short cavity using a 0.05% Cr^+ doped rod. Amplification occurs predominantly at the periphery of the rod. (b) Same for a 0.03% Cr^+ doped rod. Amplification occurs homogeneously over the rod cross section.

They are measured in the vicinity of the output of the short cavity laser (rear mirror—glasses, Fig. 2, item 6); the spread of the laser energy across the beam is very homogeneous for the low-dope rod. As a result, about 90% of the scattered energy is concentrated within a 3.5 mm spot at the plasma center and within a ~6 mm spot at the plasma edge ($z=\pm 450$ mm). Furthermore, the application of the low-dope ruby improved the pumping to probing efficiency significantly by more than a factor of 1.5. Therefore, it is expected that it is feasible to generate multiple (up to four) bursts with a time separation of >0.5 s between the bursts, each with a pulse train starting with energy of more than 15 J.

IV. MULTIPULSE DETECTION SYSTEM

Behind the tokamak window, scattered light is collected by a multielement viewing lens and guided to a Littrow spectrometer (Fig. 6) via a 28 m long coherent fiber bundle for observation of the full plasma diameter. At the input side the fiber array consists of 600×3 fibers, converted to 300×6 at the output side. For the edge observation a coherent bundle of 98×3 fibers is installed. Light, which enters the 260 mm high entrance slit of the spectrometer, is dispersed by a grating in Littrow setup. Using a motor controlled rotation table, different kinds of gratings can be selected covering different temperature ranges: a 600 lp/mm for $100\ \text{eV}\leqslant T_e\leqslant 5$ keV, a 900 lp/mm grating for $50\ \text{eV}\leqslant T_e\leqslant 2$ keV, and a 1500 lp/mm grating for $5\ \text{eV}\leqslant T_e\leqslant 500$ eV especially for edge TS.

The resulting spectral image of 260×200 mm^2 is projected onto the cathode of a Gen III image intensifier, giving

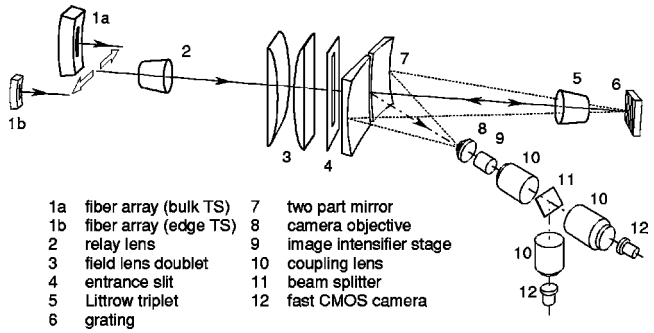

FIG. 6. Layout of the Littrow spectrometer.

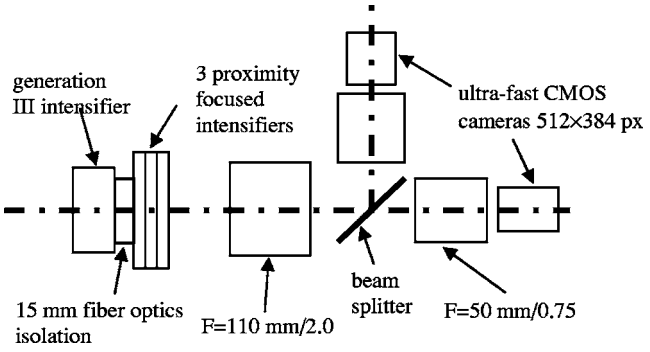

FIG. 7. Ultrafast detector. Spectrally resolved light is detected by a gated Gen III image intensifier and subsequently amplified by a stack of three proximity-focused Gen I intensifiers.

an image of 23.4×18 mm^2. A tandem lens system in combination with a beam splitter images the P46 phosphor screen onto the CMOS chips of two ultrafast cameras with magnification $M=0.45$ (see Fig. 7). One camera is used for detection of the Thomson scattered light up to 10 kHz, whereas the other is applied for measuring the plasma light between subsequent laser pulses. The magnification of the coupling lens is chosen such that the image of the two-part mirror (10.6×8.1 mm^2) is well within the chip dimensions (11.3×8.45 mm^2). The rather low gain of the Gen III intensifier and the sensitivity of the chosen CMOS camera require additional light amplification. For that purpose, a stack of three proximity-focused intensifiers is used.[8] The properties of the fast CMOS cameras and the image intensifier booster stage are described in more detail in the following subsections.

A. Ultrafast camera

The requirements for the ultrafast camera(s) are very high. Both Thomson scattering and plasma light need to be recorded at the maximum rate of the laser. That means a total frame rate of 20 000 images/s should be captured with an image format of at least 250×250 pixels. The effective dynamic range should be 8 bits or higher. This requirement implies that the maximum recordable signal should be $\geqslant 256$ times larger than twice the rms noise of the detector, which means that statistically 95% of the noise is within one count of an 8 bit system. Two different types of cameras were tested: (1) CCD cameras with on-chip storage of the images and (2) CMOS cameras, which perform fast readout of each image and storage in a random access memory (RAM).

(1) Ultrafast recording of subsequent images is possible with a CCD camera using on-chip storage of several images. A mask is used to blind off the storage area, leaving a pattern of regularly distributed light-sensitive pixels. The number of stored images depends on the applied mask and is about 4–17 (extended to 68 using a four-way beam splitter), depending on the type of the CCD camera used. Recording speed is determined by the clock rate of the CCD chip, giving frame rates up to 500 kHz. The main disadvantage of on-chip storage is the cross talk between images in the time domain. This is due to blooming effects on the CCD chip and halo of the image intensifiers applied for gating. Several cameras were tested and the cross talk between the signals of

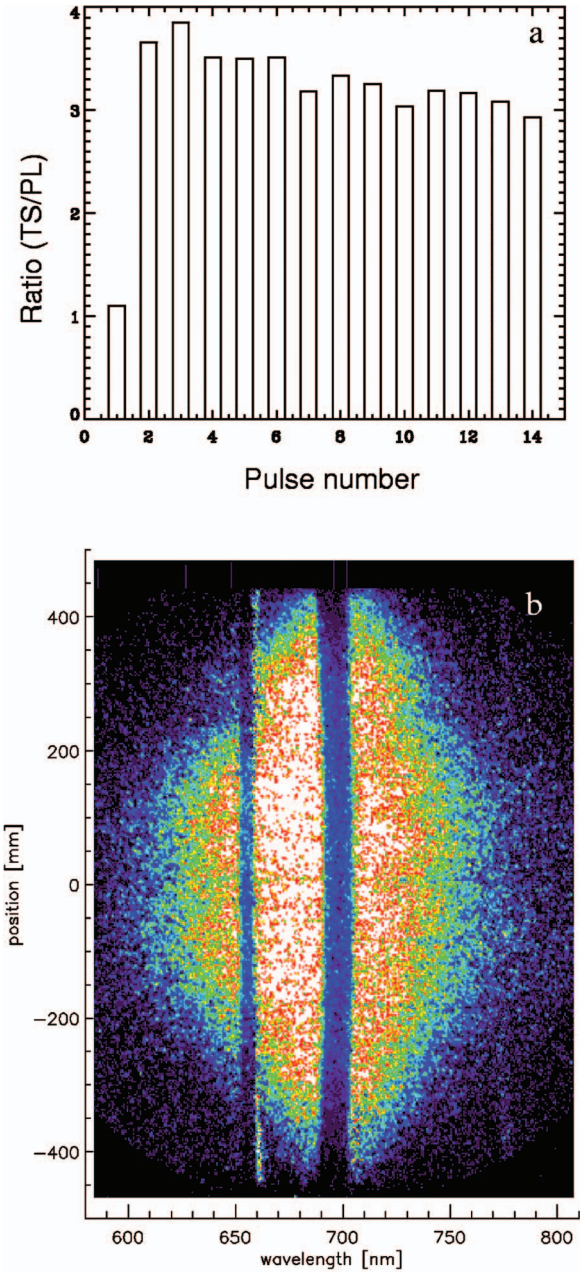

FIG. 8. (Color) (a) Measured TS/PL ratio as a function of laser pulse number. (b) Image of the TS signal after subtraction of PL background, corresponding to the second pulse in (a).

subsequent images appeared to be 1%–2% per stored image, resulting in an accumulated image-to-image cross talk of up to 15% (in case of 17 storage pixels).

(2) Several CMOS cameras were tested on rms noise, linearity, blooming of the chip, cross talk of subsequent images, shutter on-off ratio (parameter for pixel shutter quality, not described here), and sensitivity. For all cameras tested during the design phase, no blooming on chip and no cross talk could be found ($\leqslant 10^{-5}$). Linearity of the chips is well within the specified dynamic range of ±3%. In general, the sensitivity of CMOS chips can vary between 1/100 and 1/4000 count/photon at 670 nm, which are rather low sensitivities compared to those of cooled CCD cameras, which have typically 1/30 count/photon. One of the main advantages of the CMOS cameras is the continuous readout and

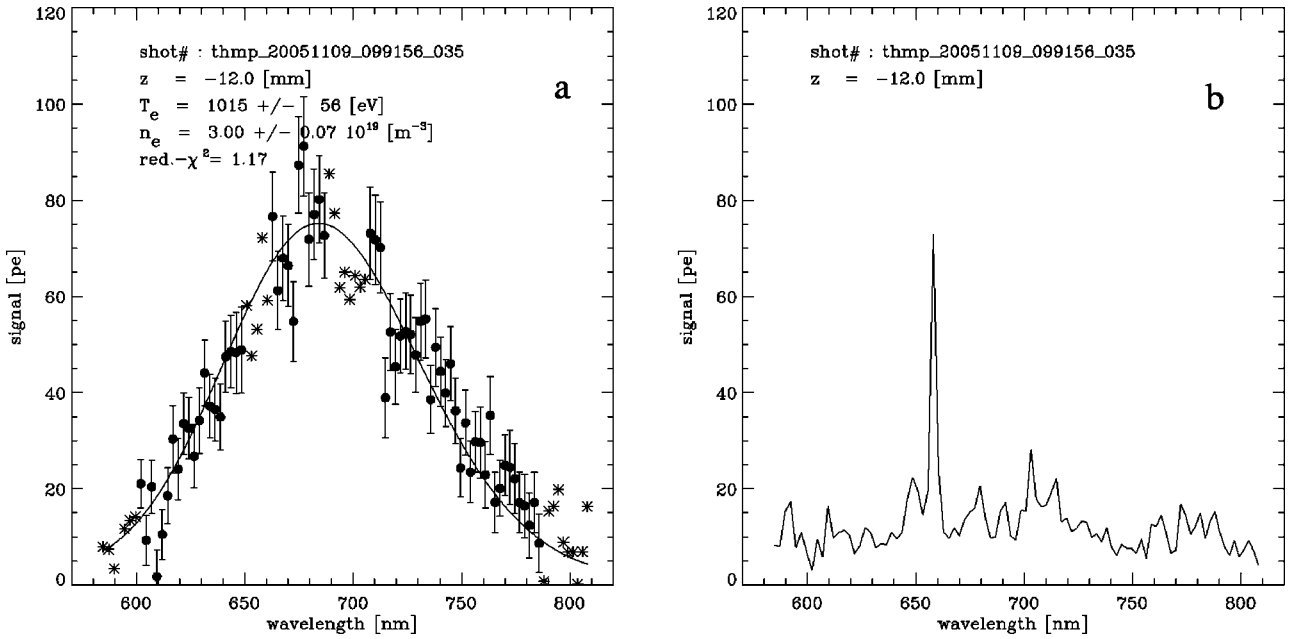

FIG. 9. (a) TS spectrum for a channel located near the equatorial plane for the same shot as in Fig. 8. Plasma light is subtracted (signal is binned over 4 pixels in wavelength and 4 pixels in the z direction). The closed circles depict the data points that are used in the fit procedure, while the data depicted by asterisks are ignored. (b) PL spectrum, used for subtraction. Some remnant H_α emission is visible due to an imperfect mask alignment at the time of measurement.

storage of images; i.e., the number of sampled images only depends on the selected image format and the capacity of the available RAM. Of all tested cameras the specifications of only one, the Phantom V7, came closest to the requirements.

The Phantom V7 can store 12 bit images of 512 $\times$384 pixels (22 μm) at a frame rate up to 10.9 kiloframes/s with a remarkably high sensitivity of $\sim$1/50 count/photon. It is found that the image-to-image cross talk of the Phantom V7 camera is only then small enough ($\sim$1.5%) when the camera is illuminated with a bias light level, corresponding to >270 counts. In that case, the detector noise is about 3 counts. As a result the effective dynamic range is 9.5 bits for a noise range of 95% probability (±6 counts). Although the Phantom V7 does not fully comply with the requested specifications, it was the best available camera at the time of purchase (2003). In a standard camera memory $\sim$3400 images of the required image format can be stored.

B. Image intensifier booster stage

Present technology of ITT Generation III intensifiers provides quantum efficiencies up to $\sim$50% over a wavelength range between 580 and 850 nm, which perfectly fits our TS application. A P46 phosphor providing a decay time of 0.2 μs is chosen to circumvent cross talk between images of subsequent laser pulses, which have a minimum separation time of 100 μs. However, a P46 phosphor has a 4–5 times lower efficiency than the P20 phosphor used in the previous double-pulse system. The maximum obtainable gain is 1300 at the maximum microchannel plate (MCP) voltage of 1150 V. To prevent electron depletion due to electron exhaust of the Gen III MCP, a MCP voltage of 990 V is used (G_{ph}=450).

For the complete detector a conversion factor (Q_0) is defined as the number of counts generated by one photoelectron detected from the Gen III intensifier.[9] The value of this conversion factor determines the impact of the bit and the rms detector noise on the observational error of the signal. The maximum value of Q_0 is determined by the dynamic range of the CMOS camera and the maximum electron density $n_e \leqslant 1\times10^{20}$ m^{-3}, at which $N_{\mathrm{pe}} \approx 2\times10^4$ photoelectrons (pe) are distributed over one spectrum with a height of *zbin* pixels (corresponding to $\Delta L \approx 7.5$ mm in the plasma). Assuming a half-width of TS spectrum of *wpixel* unbinned wavelength pixels, the amplitude of the TS spectrum of one pixel height is given by

$$A = \frac{N_{\mathrm{pe}} Q_0}{\mathrm{wpixel} \times \mathrm{zbin}}. \tag{1}$$

For Q_0=80 counts/pe, wpixel=170 (half of the usable CMOS detector width), and zbin=4, the amplitude $A \approx 2350$ counts, which is well below the maximum of 4096 counts. The photon gain needed to realize Q_0=80 counts/pe can be found from the relation between Q_0, the photon gain G_{ph}, the coupling lens efficiency T_{coupling}, the sensitivity S_{det} (1/50 count/photon), and the effective efficiency of the Gen III image intensifier, $\eta_{\mathrm{I}}(\sim 0.25)$.

TABLE I. Main parameters of the Thomson scattering system.

Energy per laser pulse	E	15 J
Solid angle	Ω	1.88×10^{-3} sr
Scattering volume (3 pixels on CMOS chip)	ΔL	6×10^{-3} m
Thomson scattering cross section	σ_T	7.94×10^{-30} m^2
Overall transmission till first photocathode	τ_{overall}	0.15
Effective quantum efficiency (QE=50%, noise figure=1.35)	$\eta_{\mathrm{intensifier}}$	0.27
Transmission through spectrometer slit	η_{slit}	0.85

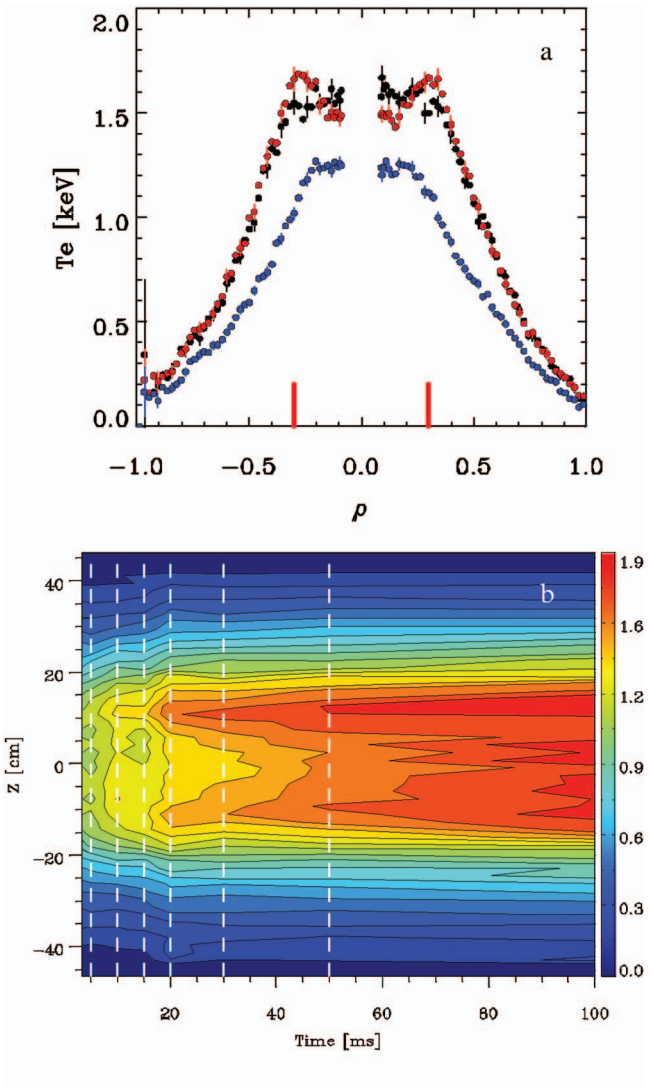

FIG. 10. (Color) (a) Electron temperature profiles in TEXTOR at 45 ms after switch-on of off-axis ECRH in an Ohmic discharge (red). The red bars indicate the ECRH deposition location. The black profile is measured after adding 300 kW Neutral Beam Injection into a similar discharge. For comparison, an Ohmic profile (blue) is also shown. The profiles are plotted vs the normalized minor radius ρ. The gap in the profile center is due to the fact that the Thomson laser is 9 cm off center with respect to the geometric axis. (b) Contour plot of the electron temperature as a function of time after ECRH switch-on. The dashed lines indicate the times of TS measurement.

$$Q_0 = \frac{G_{\mathrm{ph}} T_{\mathrm{coupling}} S_{\mathrm{det}}}{\eta_1}. \tag{2}$$

For the applied F/3 lens, a 50% beam splitter and a 95% transmission of the coupling lenses, $T_{\mathrm{coupling}}=0.013$. Inserting these values gives a required total photon gain of $G_{\mathrm{ph}} \approx 7.7\times 10^4$. Since linear operation of the Generation III intensifier is well feasible at $G_1 \sim 450$, a booster stage is needed to increase the photon gain by at least another factor of ~171. This gain could be realized with a stack of three proximity-focused intensifiers equipped with S20 cathodes and P46 screens,[8] operating at 12 kV and each with a gain of ~5.6.

V. DATA ANALYSIS

In principle, data analysis is the same as for the previous double-pulse system,[5] now executed multiple times, with two main differences.

First, to capture the TS photons during the full laser pulse the image intensifier needs to be gated for 1.8 μs. This discloses one of the main critical points of this diagnostic: the competition between the plasma background light and the TS signal. Therefore, the background is measured in addition to every laser pulse to enable correction for this.

Second, the measured TS spectrum at each position is the sum of two relativistic spectral-distribution functions, with different shapes corresponding to back- and forward scatterings. The scattering angle along the full chord of 900 mm varies between 70° and 110°. However, still a two-parameter fit (depending on T_e and n_e values) is used to describe the spectrum since a fixed ratio between the forward and backward energies can be applied.

VI. SYSTEM PERFORMANCE

The number of the detected photoelectrons can be calculated from the scattering formula:

$$N_{\mathrm{pe}} = \frac{E}{h\nu_0} \Delta L \Omega n_e \sigma_T \tau_{\mathrm{overall}} \eta_{\mathrm{intensifier}} \eta_{\mathrm{slit}}. \tag{3}$$

Using this formula in combination with the TS system parameters described in Table I results in an expected number of photoelectrons $N_{\mathrm{pe}}=2190$ at a density of $n_e=1.0\times 10^{19}$ m^{-3}. To compare this value with the measured number of photoelectrons, the conversion factor Q_0 was determined from statistical analysis of a CMOS image with a homogeneous illumination, giving $Q_0=80$ counts/pe. Using Rayleigh scattering, the system sensitivity at an energy of 15 J, $\Delta L=4$ pixels and $Q_0=80$ counts/pe, was found to be 1510 photoelectrons at a density of $n_e=1.0\times 10^{19}$ m^{-3}, which is about 30% lower than the theoretical value. The reason for this difference can be too high assumed values for the effective quantum efficiency of the image intensifier, the laser power, and/or the efficiency of the booster stage.

The expected number of detected TS photoelectrons is such that an observational error of $<3\%$ in n_e at $n_e=1.0\times 10^{19}$ m^{-3} is possible, if the background contribution from plasma light would be negligible. Although in a tokamak the plasma light background can be considerable, a simple calculation shows that very accurate measurements of n_e are achievable, provided that the integrated TS signal is more than two to three times higher than that of the plasma light (PL) signal.

Assume that $S_1=\mathrm{TS}+\mathrm{PL}$ and $S_2=\mathrm{PL}$ are the signals (in number of photoelectrons) measured during and after the laser pulse, respectively. The corrected TS signal is $S=S_1-S_2$. Using Poisson statistics, one finds the error dS in S, which can be expressed as a function of the relative error in n_e:

$$\frac{dS}{S} = \frac{dn_e}{n_e}\sqrt{1+2\mathrm{PL}/\mathrm{TS}}, \tag{4}$$

with dn_e/n_e refering to the observational error in the case when there is no plasma light at all, PL=0. The signal ratio

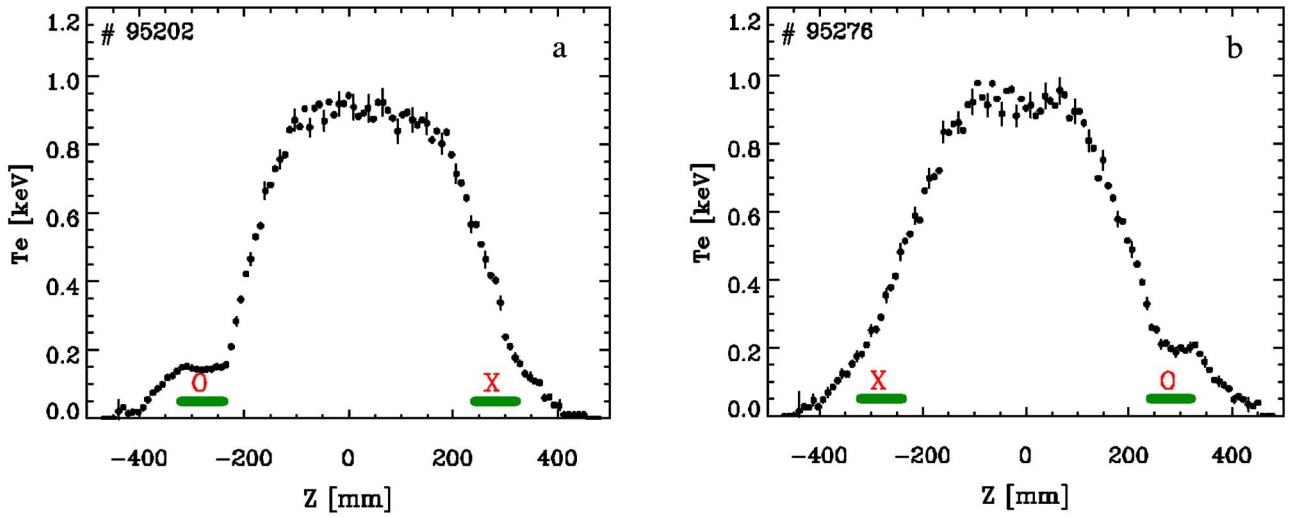

FIG. 11. (Color online) [a and b] Temperature profiles through different phases of a stationary $m/n=2/1$ magnetic island, measured in two different TEXTOR shots with static dynamic ergodic divertor (DED) operation. The island structures have a width of about 8 cm (depicted by the green lines) and are clearly seen in both shots. The profile perturbations by the islands are found to be asymmetric and are consistent with the DED coil current settings.

of TS and PL exceeds even a factor of 3.5 [see Fig. 8(a)], which implies that the plasma light background contributes less than 25% to the observational error in n_e. The image of the TS signal is shown in Fig. 8(b). The wide and narrow vertical dark bands in the image correspond to the spectral ranges near the original laser wavelength (leaving the spectrometer via the slit in the two-part mirror) and the H_α wavelength, which is blocked by a mask on the spectral mirror (Fig. 6, item 7).

VII. RESULTS

The MPTS system has come into operation late 2004, and its performance has been gradually improved since then. In this section a number of typical measurement results are given.

A measured TS spectrum, corresponding to a location near the equatorial plane in the plasma is shown in Fig. 9(a) along with the plasma light spectrum in Fig. 9(b). The solid line in Fig. 9(a) is a two-parameter spectral fit to the data. The fitted values of T_e and n_e are 1.015 ± 0.056 keV and $(3.00\pm0.07)\times10^{19}$ m^{-3}, respectively. The accuracies in the T_e and n_e determination are ~5% and ~2% for the shown spectrum, and they agree reasonably well with the target accuracies of 8% and 4%, respectively, at 10^{19} m^{-3} and 15 J laser energy.

In the early operational phase of the MPTS system, using the 0.05% doped Cr^+ rod, the pulse energy strongly degraded within a burst. For this reason it was not yet possible to follow fast processes in the plasma. However, for relatively slowly varying or stationary plasma processes it was possible to measure T_e profiles with very high accuracy. In Fig. 10(a) examples are shown of T_e profiles measured in Ohmic plasmas and at 45 ms after switch-on of off-axis electron cyclotron resonance heating (ECRH), in an Ohmic plasma and in a plasma with low-power neutral beam injection, respectively. The data from 12 individual pulses within a single burst were summed and the equivalent laser energy that was used per profile was typically ~220 J. The gap in the profile (plotted versus normalized plasma radius ρ) is due to the fact that the Thomson viewing line crosses the plasma 9 cm towards the low field side of the geometric axis. So the actual plasma center is not seen. Figure 10(b) gives a contour plot of the T_e profile versus time relative to off-axis ECRH switch-on. Here the vertical axis is the position along the Thomson laser chord. The times of Thomson measurements (except for one at 100 ms) are indicated by vertical dashed lines. The data have been interpolated. The very pronounced hollow shape of the T_e profile during application of off-axis ECRH in an Ohmic discharge is explained by the fact that the Ohmic input power in the plasma core drops below the power lost by the electrons due to collisions with ions.[10,11]

Summing data from consecutive laser pulses within a burst has also been used to study the T_e profiles in TEXTOR plasmas with a pronounced $m/n=2/1$ magnetic island [see Fig. 11(a) and 11(b)]. In these plasma the dynamic ergodic divertor (DED) was operated in the static mode, which led to a complete locking of the island. Depending on the phasing through the DED coils, the island could be locked such that the TS laser chord crosses the X point at the top of the plasma, while still crossing through the (edge of the) island itself at the bottom and the other way around. As evident from Fig. 11 the electron temperature inside the island is rather flat.[10,12]

The real demonstration of the merits of the TEXTOR MPTS system came from plasmas with rotating $m/n=2/1$ islands (see Fig. 12). The measurements in Fig. 12 were taken after installation of the 0.03% doped Cr^+ rod with a repetition rate of 5 kHz (measurement times are indicated by the vertical dashed lines). A very strong density peaking is evident inside the island, while—as in Fig. 11—the electron temperature inside the island is flattened.[10] Measurementssuch as the one plotted in Fig. 12 are now used to study the dynamics of $m/n=2/1$ mode suppression in TEXTOR via ECRH and electron cyclotron current drive.

With the edge observation system, measurements have

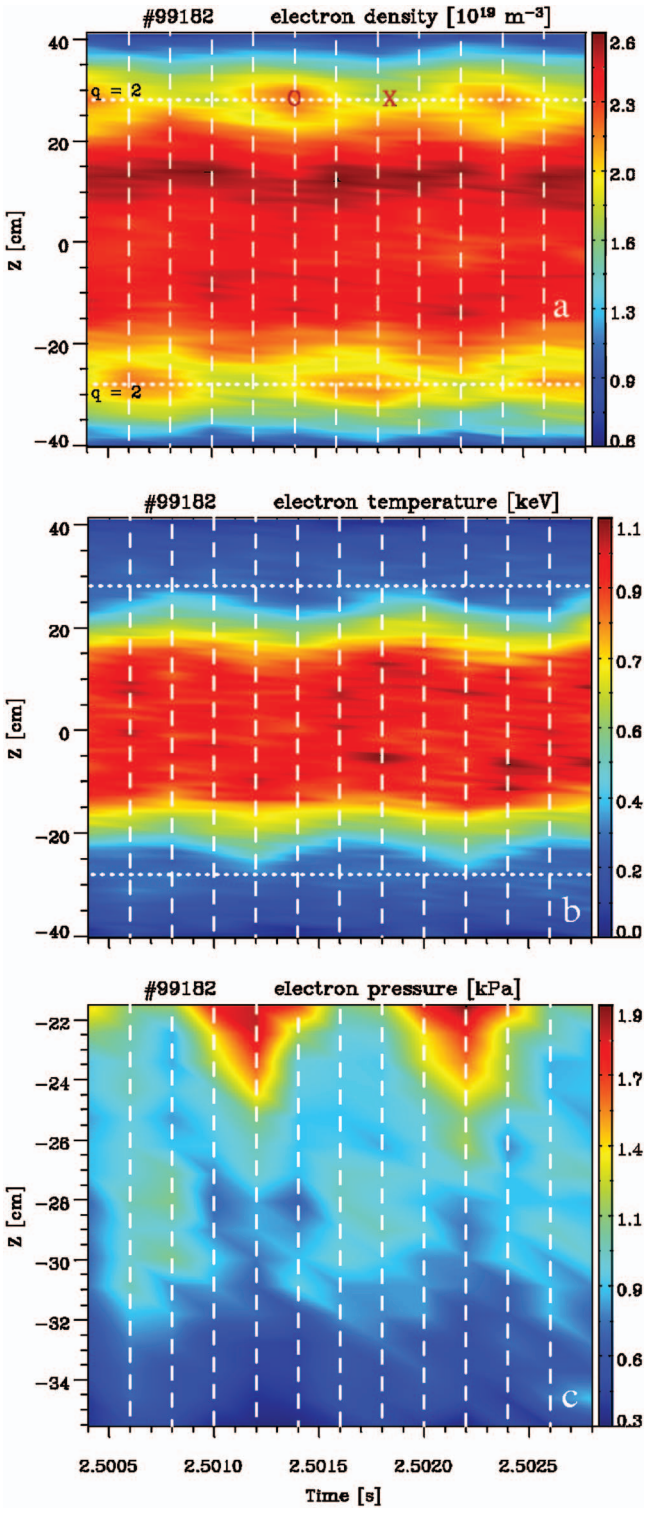

FIG. 12. (Color) Dynamics of a rotating $m/n=2/1$ magnetic island made visible by the contour plots of (a) electron density, (b) electron temperature, and (c) pressure profiles measured with high-resolution multipulse Thomson scattering system at TEXTOR. The peaking of density and flattening of temperature within the *O* point of the island is evident. The horizontal lines indicate the location of the $q=2$ surface. The vertical lines indicate time points of profile measurement. The measurements have been done in a single discharge at 5 kHz repetition rate.

been done on modifications in the edge temperature and density gradients during passage of edge localized modes (ELMs) in *H*-mode discharges. These data are presently subject to analysis and cannot yet be reported here.

VIII. SUMMARY AND PERSPECTIVES

After the application of the low-dope ruby rod, the expected statistical error at $n_e \sim 2.5\times 10^{19}$ m^{-3} on T_e and n_e for 50 eV$\leqslant T_e \leqslant$2 keV became ~8% and 4%, respectively for the full chord observation. For edge observations the expected observational errors on T_e and n_e are ~8% and 4%, respectively at $n_e \sim 10^{19}$ m^{-3}, a temperature range of 5–500 eV, and an assumed laser energy of 15 J. The edge TS observation system is ready for operation. It will, combined with the TEXTOR dynamic ergodic divertor, provide detailed information about electron dynamics in the outer region of the plasma.

The relatively high repetition rate of the TS system enables the study of electron dynamics in hot plasmas. Examples of this have been given in Sec. VII. Thus far the system has been operated with a single CMOS camera (measuring alternatingly the Thomson scattered and the plasma light) and the laser operating at 5 kHz. Operation of the laser at 10 kHz, albeit at somewhat lower power levels, has already been achieved in a mock up at the Ioffe Institute. In the very near future the operation of the MPTS system will be extended to three to four bursts (of typically 20–30 pulses each at 10 kHz repetition rate). A critical issue in this respect will be the effect of thermal lensing of the ruby rod. In case this becomes significant, a possible solution would be to include phase contrast mirrors in the system.[13] The system is already planned to be used for studies of edge localized modes in *H* modes, DED-induced structures in the edge plasma, disruptions, and internal transport barriers.

ACKNOWLEDGMENTS

This work, supported by the European Communities under the contracts of the Association EURATOM/FOM and EURATOM/FZJ, was carried out within the framework of the European Fusion Programme with financial support from NWO, the "Innovationsfond" of the Forschungszentrum Jülich, and NWO-RFBR Grant No. 047.016.015.

[1] N. Bretz, D. Dimock, V. Foote, D. Johnson, D. Long, and E. Tolnas, Appl. Opt. **17**, 192 (1978).
[2] C. J. Barth *et al.*, Rev. Sci. Instrum. **68**, 3380 (1997).
[3] C. J. Barth, F. J. Pijper, H. J. van der Meiden, J. Herranz, and I. Pastor, Rev. Sci. Instrum. **70**, 763 (1999).
[4] C. J. Barth, H. J. van der Meiden, T. Oyevaar, and N. J. Lopes Cardoza, Rev. Sci. Instrum. **72**, 1138 (2001).
[5] M. Yu. Kantor, C. J. Barth, D. V. Kouprienko, and H. J. van der Meiden, Rev. Sci. Instrum. **72**, 1159 (2001).
[6] More information about this subject is given in the test report, M. Yu. Kantor and D. V. Kouprienko, "On a Pilot Experiment for Multipass Intracivity TS on TEXTOR," 2000 (unpublished).
[7] H. J. van der Meiden *et al.*, Rev. Sci. Instrum. **75**, 3849 (2004).
[8] Assembled by Lambert Instruments, The Netherlands.
[9] C. J. Barth, C. C. Chu, M. N. A. Beurskens, and H. J. van der Meiden, Rev. Sci. Instrum. **72**, 3514 (2001).
[10] S. K. Varshney, Ph.D. thesis, Eindhoven University of Technology, 2006.
[11] S. K. Varshney *et al.*, Proceeding of the 12th International Symposium on Laser-Aided Plasma Diagnostics, Snowbird, USA, 2005 (unpublished), CD-ROM.
[12] S. K. Varshney *et al.*, Europhys. Conf. Abstr. **28G**, p-1.127 (2004).
[13] T. Hatae, O. Naiot, M. Nakatsuka, and H. Yoshida, Rev. Sci. Instrum., these proceedings.